

Analysis of flux-integrated cross sections for quasi-elastic neutrino charged-current scattering off ^{12}C at MiniBooNE energies.

A. V. Butkevich

*Institute for Nuclear Research, Russian Academy of Sciences,
60th October Anniversary Prosp. 7A, Moscow 117312, Russia*

(Dated: October 27, 2018)

Flux-averaged and flux-integrated cross sections for quasi-elastic neutrino charged-current scattering on nucleus are analyzed. It is shown that the flux-integrated differential cross sections are nuclear model-independent. We calculate these cross sections using the relativistic distorted-wave impulse approximation and relativistic Fermi gas model with the Booster Neutrino Beamline flux and compare results with the recent MiniBooNE experiment data. Within these models an axial mass M_A is extracted from a fit of the measured $d\sigma/dQ^2$ cross section. The extracted value of M_A is consistent with the MiniBooNE result. The measured and calculated double differential cross sections $d\sigma/dTd\cos\theta$ generally agree within the error of the experiment. But the Fermi gas model predictions are completely off of the data in the region of low muon energies and scattering angles.

PACS numbers: 25.30.-c, 25.30.Bf, 25.30.Pt, 13.15.+g

I. INTRODUCTION

The current [1–4] and planned [5] set of accelerator-based neutrino experiments use extremely intense neutrino beamlines for precise measurements of the observed neutrino mass splitting and mixing angles and detailed experimental study of the neutrino mixing matrix. The data of these experiments will greatly extend the statistics due to extremely intense neutrino beamline.

In this situation, the statistical uncertainties should be negligible as compared to systematic errors. An important source of systematic uncertainties is related to the neutrino-nucleus (νA) cross sections. The neutrino beams of high intensity cover the few-GeV energy range. In this energy regime, the dominant contribution to νA cross section comes from

charged-current (CC) quasielastic (QE) scattering and resonance production processes. In the long-baseline neutrino oscillation experiments near and far detectors are used to normalize the neutrino flux at production and to search for the neutrino oscillation effects. While many unknown quantities are eliminated in these experiments by considering ratios of far to near events, the cancellation is not complete due to differences in neutrino flux and backgrounds in the near and far detectors. Thus, in order to permit precision oscillation measurements it is important to have an accurate characterization of the CCQE differential cross sections over wide span neutrino energies.

The current data on CCQE scattering come from a variety of experiments operating at differing energies and with different nuclei. The existing data on (anti)neutrino CCQE scattering come mostly from bubble chamber experiments, which suffer from small statistics. In general, the experimental execution and data interpretation are non-trivial for several reasons. Neutrino beams typically span a wide energy range. The neutrino flux itself is often poorly known and a background from resonance processes are frequently significant and it is difficult for separating from the CCQE signal. Therefore the total QE cross sections measured in different experiments with accuracy of 20-40% and even within such large uncertainties some results contradict each other. The difference between the total quasielastic cross sections, calculated within the framework of various models [8–20] is lower than the spread in data.

More information about neutrino-nuclear CCQE interaction can be obtained from the analysis of the charged-current QE event distributions and $d\sigma/dQ^2$ differential cross sections as functions of Q^2 (squared four-momentum transfer) [21]. The shape of these distributions is sensitive to the Q^2 dependence of two vector, $F_{1,2}(Q^2)$, one axial-vector $F_A(Q^2)$ form factors and nuclear effects. The vector form factors are well-known from electron scattering. For the axial-vector form factors the dipole parametrization with one free parameter M_A (axial mass) is mainly used. This parameter controls the Q^2 dependence of $F_A(Q^2)$, and ultimately, the normalization of the predicted cross sections. The dipole parametrization has no strict theoretical basis and the choice of this parametrization is made by the analogy with electroproduction. To describe the nuclear effects, neutrino CCQE models typically employ a relativistic Fermi gas model (RFGM) [8] in which the nucleons with a flat nucleon momentum distribution up to the same Fermi momentum p_F and nuclear binding energy ϵ_b . The experimental values of M_A extract from the (anti)neutrino CCQE scattering data, i.e.

from the analysis of the shape of the Q^2 -distributions and from the direct measurements of the total cross sections. They show very wide spread from roughly 0.7 to 1.2 GeV and the resulting world-average $M_A = 1.03 \pm 0.02$ GeV [22].

Several experiments have recently reported new results on CCQE scattering from high-statistics data samples with intense, well-understood neutrino beams. The NOMAD experiment [23] observe an M_A value and cross section (from data taken on carbon) consistent with prior world-average. However, data of [1, 24–26] and [27] (preliminary result), collected on carbon, oxygen, and iron targets, have indicated a somewhat larger value for M_A (by $\approx 10 - 30\%$). In these experiments the shape of the Q^2 -distribution was analyzed.

This data show a disagreement with the RFGM predictions. The data samples exhibit deficit in the region of low $Q^2 \leq 0.2$ (GeV/c)² (so-called low- Q^2 problem). As it is known the comparison with the low-energy QE electron-nucleus scattering data, the RFGM description of this region is not accurate enough [28]. In the region of high- Q^2 the data excess is observed, and value of M_A , obtained from a fit to the measured data, is higher than the results of the previous experiments. The collection of existing results remains puzzling. The next experiments MINERvA [6] and MicroBooNE [7] as well as T2K [3] and NOvA [5] near detectors will be able to make more precise measurements of the CCQE cross sections in a wide range of energies and for various nuclear targets.

The uncertainties in the theoretical description of the quasielastic neutrino-nucleus scattering could be considerably reduced if new model-independent absolute differential cross section could be provided. The first measurement of the flux-integrated double-differential cross section (in muon energy and angle) for CCQE scattering on carbon has been produced in MiniBooNE experiment [29]. This cross section contains the most complete and model-independent information that is available from MiniBooNE for the CCQE process.

The aim of this work is to test the RFGM and relativistic distorted-wave impulse approximation (RDWIA) predictions against the MiniBooNE data [29]. In the framework of these approaches we extract the values of axial mass from the measured flux-integrated $d\sigma/dQ^2$ cross section. Then, we calculate with extracted values of M_A the flux-integrated differential and flux-unfolded total cross sections and compare the results with data.

The outline of this paper is the following. In Sec. II we present briefly the RDWIA model and discuss the flux-averaged and flux-integrated differential cross sections. The results are presented in Sec. III. Our conclusions are summarized in Sec. IV.

II. MODEL, FLUX-AVERAGED AND FLUX-INTEGRATED DIFFERENTIAL CROSS SECTIONS

We consider neutrino charged-current QE exclusive

$$\nu(k_i) + A(p_A) \rightarrow \mu(k_f) + N(p_x) + B(p_B), \quad (1)$$

and inclusive

$$\nu(k_i) + A(p_A) \rightarrow \mu(k_f) + X \quad (2)$$

scattering off nuclei in the one-W-boson exchange approximation. Here $k_i = (\varepsilon_i, \mathbf{k}_i)$ and $k_f = (\varepsilon_f, \mathbf{k}_f)$ are the initial and final lepton momenta, $p_A = (\varepsilon_A, \mathbf{p}_A)$, and $p_B = (\varepsilon_B, \mathbf{p}_B)$ are the initial and final target momenta, $p_x = (\varepsilon_x, \mathbf{p}_x)$ is the ejectile nucleon momentum, $q = (\omega, \mathbf{q})$ is the momentum transfer carried by the virtual W-boson, and $Q^2 = -q^2 = \mathbf{q}^2 - \omega^2$ is the W-boson virtually.

A. Model

The formalism of charged-current QE exclusive and inclusive reactions is described in [18]. All the nuclear structure information and final state interaction effects (FSI) are contained in the weak CC nuclear tensors $W_{\mu\nu}$, which are given by bilinear product of the transition matrix elements of the nuclear CC operator J_μ between the initial nucleus state $|A\rangle$ and the final state $|B_f\rangle$ as

$$W_{\mu\nu} = \sum_f \langle B_f, p_x | J_\mu | A \rangle \langle A | J_\nu^\dagger | B_f, p_x \rangle, \quad (3)$$

where the sum is taken over undetected states.

We describe CCQE neutrino-nuclear scattering in the impulse approximation (IA), assuming that the incoming neutrino interacts with only one nucleon, which is subsequently emitted, while the remaining (A-1) nucleons in the target are spectators. The nuclear current is written as the sum of single-nucleon currents. Then, the nuclear matrix element in Eq.(3) takes the form

$$\langle p, B | J^\mu | A \rangle = \int d^3r \exp(it \cdot \mathbf{r}) \bar{\Psi}^{(-)}(\mathbf{p}, \mathbf{r}) \Gamma^\mu \Phi(\mathbf{r}), \quad (4)$$

where Γ^μ is the vertex function, $\mathbf{t} = \varepsilon_B \mathbf{q}/W$ is the recoil-corrected momentum transfer, $W = \sqrt{(m_A + \omega)^2 - \mathbf{q}^2}$ is the invariant mass, Φ and $\Psi^{(-)}$ are relativistic bound-state and outgoing wave functions.

The single-nucleon charged current has $V-A$ structure $J^\mu = J_V^\mu + J_A^\mu$. For a free-nucleon vertex function $\Gamma^\mu = \Gamma_V^\mu + \Gamma_A^\mu$ we use the CC2 vector current vertex function Γ_V^μ . The weak vector form factors are related to the corresponding electromagnetic ones for protons and neutrons by the hypothesis of the conserved vector current. We use the approximation of Ref. [31] on the nucleon form factors. Because the bound nucleons are off shell we employ the de Forest prescription [32] and Coulomb gauge for off-shell vector current vertex Γ_V^μ . The vector-axial and pseudoscalar form factors are parametrized as a dipole with the axial-vector mass, which controls the Q^2 dependence of F_A , and ultimately, the normalization of the predicted cross section.

According to the JLab data [33, 34] the occupancy of the independent particle shell-model (IPSM) orbitals of ^{12}C equals on average 89%. In this work we assume that the missing strength (11%) can be attributed to the short-range nucleon-nucleon (NN) correlations in the ground state, leading to the appearance of the high-momentum (HM) and high-energy component in the nucleon distribution in the target. To estimate this effect in the inclusive cross sections we consider a phenomenological model which incorporates both the single-particle nature of the nucleon spectrum at low energy (IPSM orbitals) and the high-energy and high-momentum components due to NN correlations.

In the independent particle shall model the relativistic wave functions of the bound nucleon states Φ are obtained as the self-consistent (Hartree–Bogoliubov) solutions of a Dirac equation, derived, within a relativistic mean field approach, from Lagrangian containing σ , ω , and ρ mesons (the $\sigma - \omega$ model)[35]. We use the nucleon bound-state functions calculated for carbon by the TIMORA code [36] with the normalization factors $S(\alpha)$ relative to the full occupancy of the IPSM orbitals of ^{12}C : $S(1p_{3/2})=84\%$, $S(1s_{1/2})=100\%$, and an average factor of about 89%. These estimations of the depletion of hole states follow from the RDWIA analysis of $^{12}\text{C}(e, e'p)$ for $Q^2 < 2$ (GeV/c) 2 [34] and are consistent with a direct measurement of the spectral function using $^{12}\text{C}(e, e'p)$ in parallel kinematics [39], which observed approximately 0.6 protons in a region attributable to a single-nucleon knockout from correlated cluster.

For the outgoing nucleon the simplest choice is to use plane-wave function Ψ , i.e., no

interactions is considered between the ejected nucleon N and the residual nucleus B (PWIA - plane-wave impulse approximation). For a more realistic description, FSI effects should be taken into account. In the RDWIA the distorted-wave function Ψ are evaluated as solution of a Dirac equation containing a phenomenological relativistic optical potential. The channel coupling in the FSI [37] of the $N + B$ system is taken into account. The relativistic optical potential consists of a real part which describes the rescattering of the ejected nucleon and of an imaginary part that accounts for absorption of it into unobserved channels.

Using the direct Pauli reduction method the system of two coupled first-order radial Dirac equations can be reduced to a single second-order Schrödinger-like equation for the upper component of Dirac wave function Ψ . We use the LEA program [38] for the numerical calculation of the distorted wave functions with the EDAD1 parametrization [40] of the relativistic optical potential for carbon. This code, initially designed for computing exclusive proton-nucleus and electron-nucleus scattering, was successfully tested against $A(e, e'p)$ data [33, 41] and we adopted this program for neutrino reactions.

A complex optical potential with a nonzero imaginary part generally produces an absorption of the flux. For the exclusive $A(l, l'N)$ channel this reflects the coupling between different open reaction channels. However, for the inclusive reaction, the total flux must conserve. In Ref. [11, 43] it was shown that the inclusive CCQE neutrino cross section of the exclusive channel $A(l, l'N)$, calculated with only the real part of the optical potential is almost identical to those of the Green's function approach [11, 42] in which the FSI effects on inclusive reaction $A(l, l'X)$ is treated by means of a complex potential and the total flux is conserved. We calculate the inclusive and total cross sections with the EDAD1 relativistic optical potential in which only the real part is included.

The inclusive cross sections with the FSI effects in the presence of the short-range NN correlations were calculated using the method proposed in Ref. [18]. In this approach the contribution of the NN correlated pairs is evaluated in the PWIA model. We use the general expression for the high-momentum and high-energy part of the spectral function from Ref. [44] with the parametrization for the nucleon high-momentum distribution from Ref. [45], which was renormalized to value of 11%. The FSI effects for the high-momentum component is estimated by scaling the PWIA cross section with $\Lambda(\varepsilon_f \Omega_f)$ function determined in Ref. [18].

B. Flux-averaged and flux-integrated differential cross sections

In neutrino experiments the differential cross sections of CCQE neutrino-nucleus scattering are measured within rather wide ranges of the (anti)neutrino energy spectrum. Therefore flux-averaged and flux-integrated differential cross sections can be extracted.

Because the ν_μ - mode of beams incorporates ν_μ and $\bar{\nu}_\mu$ spectra the flux-averaged double differential cross section $\sigma/dTd\cos\theta$ in muon kinetic energy T and muon scattering angle θ is the sum of neutrino and antineutrino cross sections

$$\left\langle \frac{d^2\sigma}{dTd\cos\theta} \right\rangle = \left\langle \frac{d^2\sigma^\nu}{dTd\cos\theta} \right\rangle + \left\langle \frac{d^2\sigma^{\bar{\nu}}}{dTd\cos\theta} \right\rangle, \quad (5)$$

where

$$\left\langle \frac{d^2\sigma^{\nu, \bar{\nu}}}{dTd\cos\theta}(T, \cos\theta) \right\rangle = \int_{\varepsilon_1}^{\varepsilon_2} W_{\nu, \bar{\nu}}(T, \cos\theta, \varepsilon_i) \frac{d^2\sigma^{\nu, \bar{\nu}}}{dTd\cos\theta}(T, \cos\theta, \varepsilon_i) d\varepsilon_i, \quad (6)$$

and $W_{\nu, \bar{\nu}}$ are weight functions. The normalization of these functions is given by

$$\int_{\varepsilon_1}^{\varepsilon_2} [W_\nu(T, \cos\theta, \varepsilon_i) + W_{\bar{\nu}}(T, \cos\theta, \varepsilon_i)] d\varepsilon_i = 1. \quad (7)$$

The weight functions are defined as follows

$$W_{\nu, \bar{\nu}}(T, \cos\theta, \varepsilon_i) = I_{\nu, \bar{\nu}}(\varepsilon_i)/\Phi(T, \cos\theta), \quad (8)$$

where $I_{\nu, \bar{\nu}}$ is the neutrino (antineutrino) spectrum in ν -mode of the flux and

$$\Phi(T, \cos\theta) = \int_{\varepsilon_1}^{\varepsilon_2} [I_\nu(\varepsilon_i) + I_{\bar{\nu}}(\varepsilon)] d\varepsilon_i \quad (9)$$

is the neutrino and antineutrino flux which give the contribution to the measured double differential cross section at the fixed values of $(T, \cos\theta)$. This flux depends on $(T, \cos\theta)$ due to the limits of integration in Eqs. (6), (7) and (9) which are functions of $(T, \cos\theta)$, i.e. $\varepsilon_i = \varepsilon_{\min}(T, \cos\theta)$ and $\varepsilon_2 = \varepsilon_{\max}(T, \cos\theta)$. In Fig. 1 the double differential cross sections, calculates within the RDWIA and RFGM (with the Fermi momentum $p_F = 221$ MeV/c and a binding energy $\epsilon_b = 25$ MeV for carbon) are shown as functions of neutrino energy. Apparently the ranges $[\varepsilon_{\max}(T, \cos\theta) - \varepsilon_{\min}(T, \cos\theta)]$ where $d\sigma^2/dTd\cos\theta$ is not equals to zero are different in the RDWIA and RFGM. Therefore the value of $\Phi(T, \cos\theta)$ is model-dependent and ultimately the weight functions and the cross section $\langle d^2\sigma/dTd\cos\theta \rangle$ depend on nuclear models too. Note that the flux $\Phi(T, \cos\theta)$ should be used to extract the measured

flux-averaged cross section in the i, j -bins of $(T, \cos \theta)$ variables (for example see Eq.(3) in Ref. [29]).

Similarly, the flux-averaged $d\sigma/dQ^2$ cross section can be written as sum

$$\left\langle \frac{d\sigma}{dQ^2} \right\rangle = \left\langle \frac{d\sigma^\nu}{dQ^2} \right\rangle + \left\langle \frac{d\sigma^{\bar{\nu}}}{dQ^2} \right\rangle, \quad (10)$$

where

$$\left\langle \frac{d\sigma^{\nu, \bar{\nu}}}{dQ^2}(Q^2, T_{th}) \right\rangle = \int_{\varepsilon_1}^{\varepsilon_2} W_{\nu, \bar{\nu}}(Q^2, \varepsilon_i) \frac{d\sigma^{\nu, \bar{\nu}}}{dQ^2}(Q^2, T_{th}, \varepsilon_i) d\varepsilon_i, \quad (11)$$

and T_{th} is the muon threshold energy after all cuts for CCQE events selection. The weight functions in Eq. (11) are defined as follows

$$W_{\nu, \bar{\nu}}(Q^2, \varepsilon_i) = I_{\nu, \bar{\nu}}(\varepsilon_i)/\Phi(Q^2), \quad (12)$$

where

$$\Phi(Q^2) = \int_{\varepsilon_1}^{\varepsilon_2} [I_\nu(\varepsilon_i) + I_{\bar{\nu}}(\varepsilon)] d\varepsilon_i \quad (13)$$

is the neutrino and antineutrino flux which gives the contribution to the measured cross section at the fixed value of Q^2 . The flux is a function of Q^2 because $\varepsilon_1 = \varepsilon_{min}(Q^2)$ and $\varepsilon_2 = \varepsilon_{max}$, where ε_{max} is the maximal energy in the (anti)neutrino spectrum. The limit $\varepsilon_{min}(Q^2)$, and ultimately the flux $\Phi(Q^2)$ depend on nuclear model. As a result the extracted flux-averaged cross section $\langle d\sigma/dQ^2 \rangle$ is model-dependent too.

In Eq.(11) the cross section $d\sigma/dQ^2$ is defined as

$$\frac{d\sigma}{dQ^2}(Q^2, T_{th}, \varepsilon_i) = \int_{\omega_{min}}^{\omega_{cut}} \frac{d^2\sigma}{dQ^2 d\omega}(Q^2, \omega) d\omega, \quad (14)$$

where $\omega_{cut} = \min\{\omega_{max}(Q^2), \varepsilon_i - m_\mu - T_{th}\}$, m_μ is the muon mass, $\omega_{max}(Q^2)$ and $\omega_{min}(Q^2)$ are the limits of the kinematic allowed ω -range at the fixed value of Q^2 . If $T_{th} = 0$ the upper limit $\omega_{cut} = \omega_{max}(Q^2)$. So, the flux-averaged differential $\langle d\sigma^2/dT d\cos\theta \rangle$ and $\langle d\sigma/dQ^2 \rangle$ cross sections are model-dependent.

In Ref. [29] the differential cross sections were extracted using the flux Φ_{BNB} that was determined by integration the Booster Neutrino Beamline flux [46] over $0 \leq \varepsilon_i \leq 3$ GeV, i.e. Φ_{BNB} is a single number ($2.90 \times 10^{11} \nu_\mu/cm^2$). Therefore, these flux-integrated differential cross sections are not model-dependent and can be written as follows

$$\left(\frac{d^2\sigma}{dT d\cos\theta} \right)^{int} = \left(\frac{d^2\sigma^\nu}{dT d\cos\theta} \right)^{int} + \left(\frac{d^2\sigma^{\bar{\nu}}}{dT d\cos\theta} \right)^{int}, \quad (15)$$

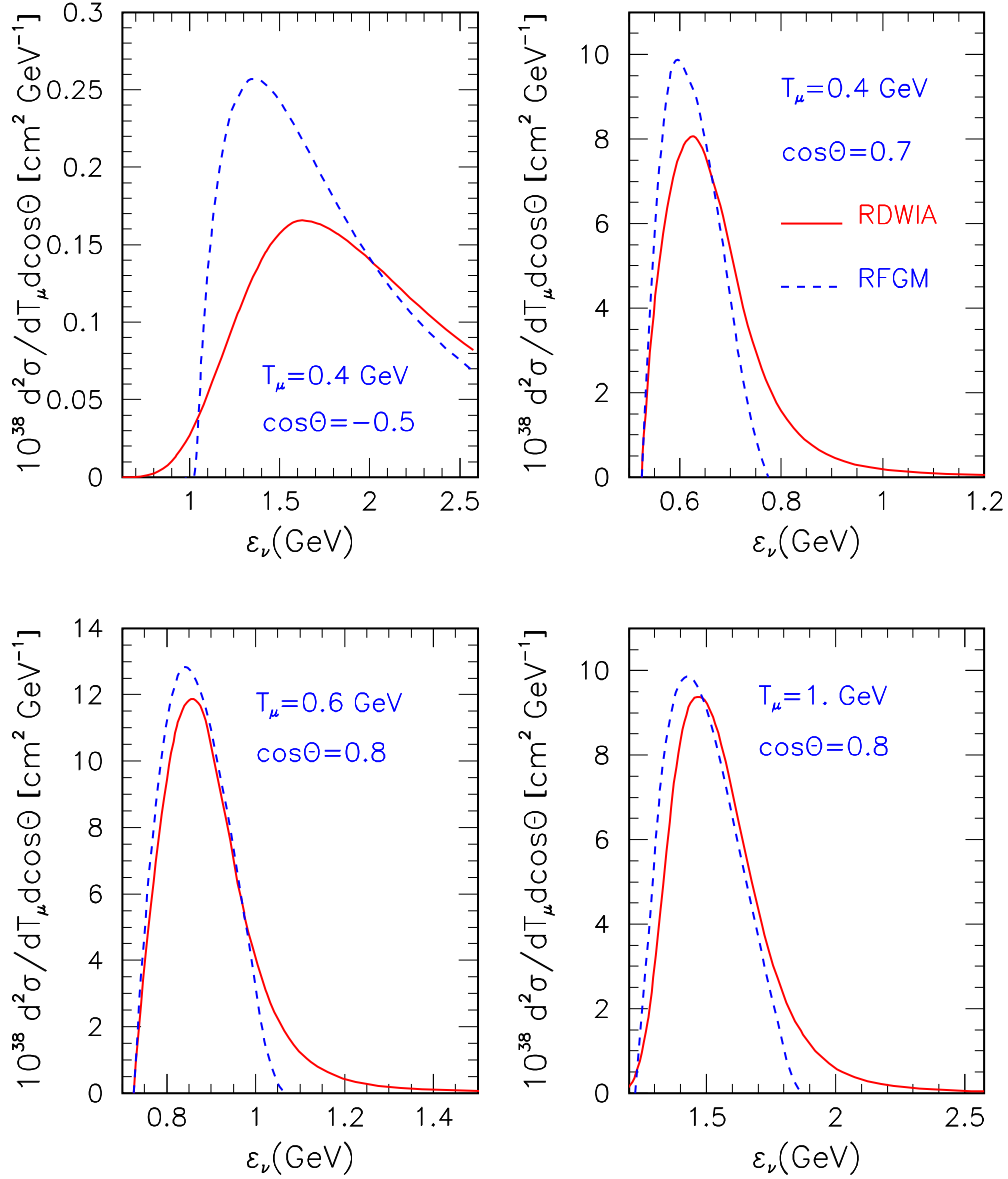


FIG. 1: (Color online) Double differential cross sections vs the neutrino energy calculated in the RDWIA (solid line) and RFGM (dashed line) approaches for the four values of $(T, \cos\theta)$: (0.4 GeV, -0.5), (0.4 GeV, 0.7), (0.6 GeV, 0.8), and (1 GeV, 0.8).

where

$$\left(\frac{d^2\sigma^{\nu, \bar{\nu}}}{dT d\cos\theta}(T, \cos\theta) \right)^{int} = \int_{\varepsilon_1}^{\varepsilon_2} \widetilde{W}_{\nu, \bar{\nu}}(T, \cos\theta, \varepsilon_i) \frac{d^2\sigma^{\nu, \bar{\nu}}}{dT d\cos\theta}(T, \cos\theta, \varepsilon_i) d\varepsilon_i, \quad (16)$$

and

$$\left(\frac{d\sigma}{dQ^2} \right)^{int} = \left(\frac{d\sigma^\nu}{dQ^2} \right)^{int} + \left(\frac{d\sigma^{\bar{\nu}}}{dQ^2} \right)^{int}, \quad (17)$$

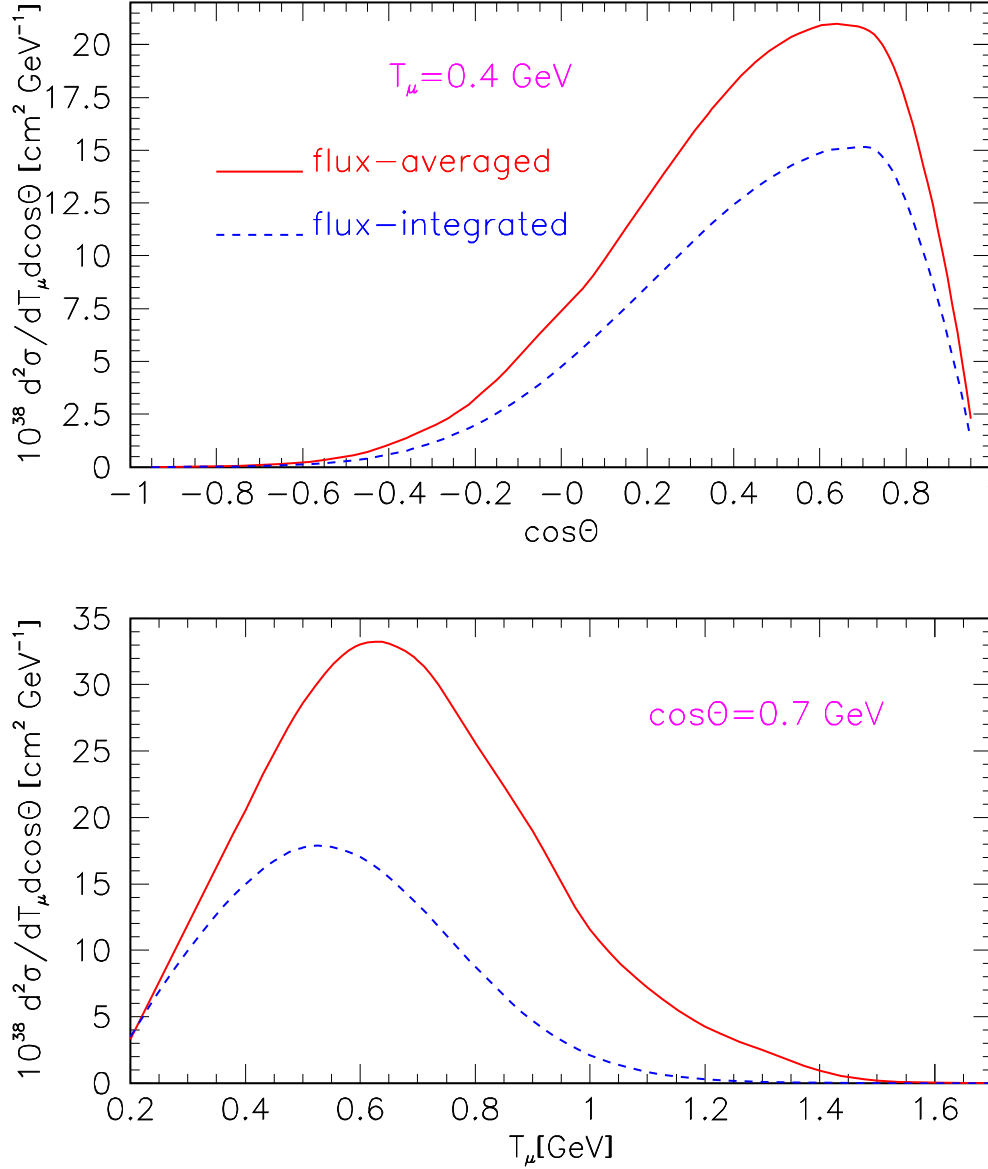


FIG. 2: (Color online) Flux-averaged (solid line) and flux-integrated (dashed line) double differential cross sections versus $\cos \theta$ for $T = 0.4 \text{ GeV}$ (upper panel) and versus T for $\cos \theta = 0.7$ (lower panel) calculated in the RDWA approach for ν - mode of the BNB flux.

where

$$\left(\frac{d\sigma^{\nu, \bar{\nu}}}{dQ^2}(Q^2, T_{th}) \right)^{int} = \int_{\varepsilon_1}^{\varepsilon_2} \widetilde{W}_{\nu, \bar{\nu}}(Q^2, \varepsilon_i) \frac{d\sigma^{\nu, \bar{\nu}}}{dQ^2}(Q^2, T_{th}, \varepsilon_i) d\varepsilon_i. \quad (18)$$

The weight functions $\widetilde{W}_{\nu, \bar{\nu}}$ are defined as

$$\widetilde{W}_{\nu, \bar{\nu}}(T, \cos \theta, \varepsilon_i) = I_{\nu, \bar{\nu}}(\varepsilon_i) / \Phi_{BNB}, \quad (19)$$

and

$$\int_{\varepsilon_1}^{\varepsilon_2} [\widetilde{W}_\nu(T, \cos\theta, \varepsilon_i) + \widetilde{W}_{\bar{\nu}}(T, \cos\theta, \varepsilon_i)] d\varepsilon_i \leq 1. \quad (20)$$

because of $\Phi_{BNB} \geq \Phi(T, \cos\theta)$ and $\Phi_{BNB} \geq \Phi(Q^2)$. These functions depend only on (anti)neutrino energy and are model-independent. As an example, on Fig. 2 the flux-averaged and flux-integrated double differential cross sections calculated within the RDWIA model for ν - mode of the BNB flux are compared. Apparently the flux-averaged cross sections are higher than the flux-integrated ones. This is because the normalization of $\widetilde{W}_{\nu, \bar{\nu}}$ (Eq.(20)) is less than unit. From the practical point of view, the flux-integrated differential cross sections are more useful than flux-averaged ones because they are not model-dependent and can be used for comparison to models of CCQE interaction on nuclear targets.

III. RESULTS AND ANALYSIS

A. CCQE flux-integrated $d\sigma/dQ^2$ differential cross section

New data for CCQE events Q^2 -distribution measured in the MiniBooNE experiment were presented in Refs. [29, 30]. The CC one pion production ($CC1\pi^+$) background was measured and subtracted instead of calculated one [1]. With measured $CC1\pi^+$ background incorporated, a “shape-only” fit to the CCQE events sample was performed to extract values for adjusted CCQE model parameters, M_A and κ within the Fermi gas model. To tune this model to the low Q^2 , the parameter κ was introduced [1] which reduced the phase space volume at low-momentum transfer. Note that at $\kappa = 1$ the phase space volume is the same as well as in the “standard” RFGM. This parameter controls the Q^2 - distribution only in the low- Q^2 region. The shape-only fit yields the model parameters, $M_A = 1.35 \pm 0.17 \text{ GeV}/c^2$ and $\kappa = 1.007 \pm 0.012$. The extracted value for M_A is approximately 30% higher than the world averaged one.

The MiniBooNE ν_μ CC flux-integrated single differential cross section $d\sigma/dQ^2$ per neutron was extracted as a function of Q^2 in the range $0 \leq Q^2 \leq 2$ (GeV/c)². To extract value for the parameter M_A we calculated this cross section with the BNB flux in the RDWIA and RFGM models using the Q^2 -bins $\Delta Q^2 = Q_{i+1}^2 - Q_i^2$ similar to Ref. [29]

$$\left(\frac{d\sigma}{dQ^2} \right)_i^{int} = \frac{1}{\Delta Q^2} \int_{Q_i^2}^{Q_{i+1}^2} \left[\frac{d\sigma}{dQ^2}(Q^2) \right]^{int} dQ^2 \quad (21)$$

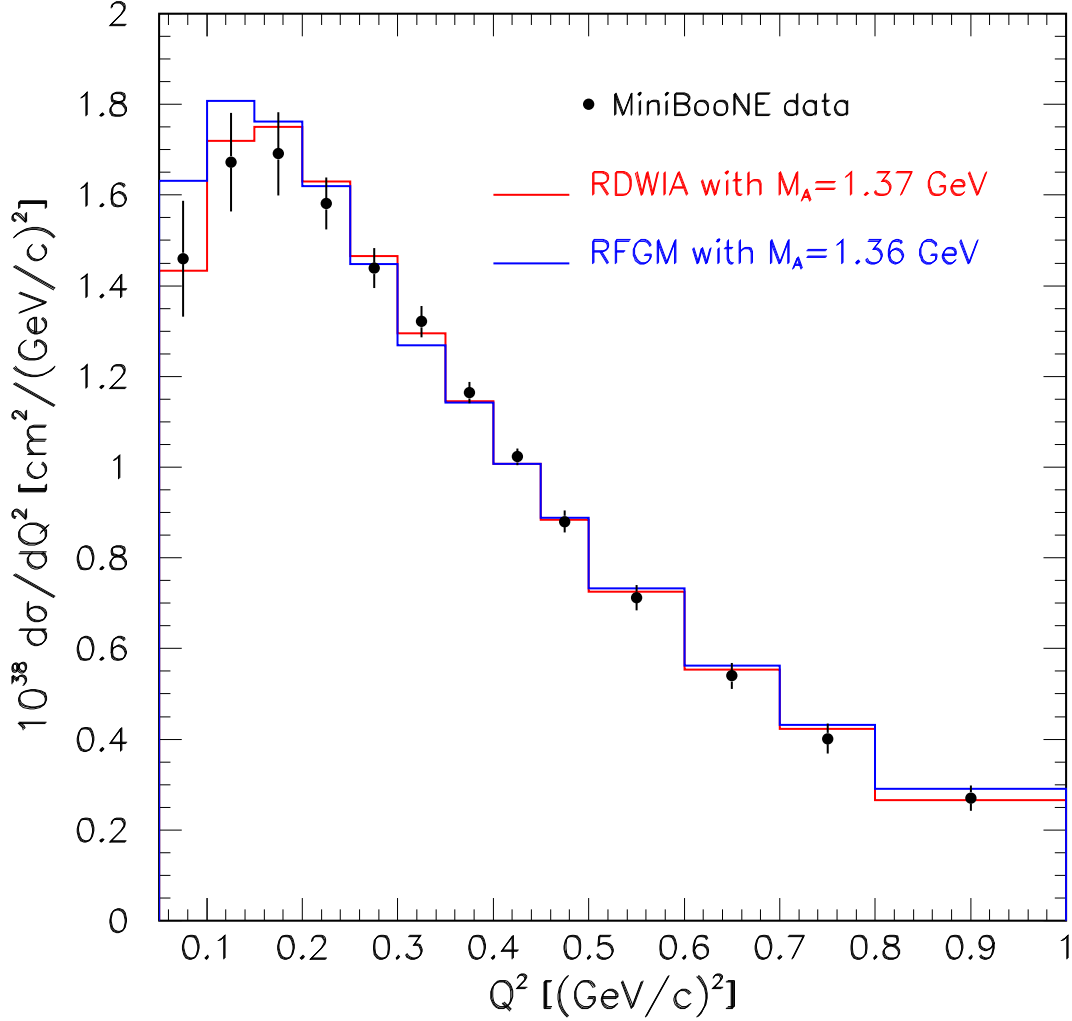


FIG. 3: (Color online) Flux-integrated $d\sigma/dQ^2$ cross section per neutron target for the ν_μ CCQE scattering. Calculations from the RDWIA with $M_A = 1.37$ GeV/ c^2 and RFGM with $M_A = 1.36$ GeV/ c^2 . The MiniBooNE data are shown as points with the shape error only.

Because the data include events with $T_\mu \leq 200$ MeV [29], we calculated $d\sigma/dQ^2$ with $T_\mu = 0$ in Eq. (14). Within the RDWIA (RFGM) model the fit to the extracted flux-integrated $d\sigma/dQ^2$ cross section with only-shape error yields the parameter $M_a = 1.37 \pm 0.05$ GeV/ c^2 ($M_A = 1.36 \pm 0.05$ GeV/ c^2). These values are consistent with the MiniBooNE result $M_A = 1.37 \pm 0.17$ GeV/ c^2 .

Figure 3 shows measured flux-integrated $d\sigma/dQ^2$ differential cross section as a function of Q^2 compared with the RDWIA ($M_A = 1.37 \text{ GeV}/c^2$) and RFGM ($M_A = 1.36 \text{ GeV}/c^2$) calculations. There is an overall agreement between the RDWIA result and the data across of the full range $Q^2 = 0 \pm 1 \text{ (GeV}/c^2)$, whereas the RFGM overestimates the measured differential cross section at $Q^2 \leq 0.2 \text{ (GeV}/c^2)$. At higher Q^2 a good match between the RFGM calculated and measured cross sections is observed. Thus, so-called low- Q^2 problem is successfully solved in the distorted-wave approach.

B. CCQE flux-integrated double differential cross section

The flux-integrated double differential cross section per neutron $d^2\sigma/dTd\cos\theta$, for the ν_μ CCQE process was extracted in Ref. [29] for the kinematic range, $-1 < \cos\theta < 1$, $0.2 < T < 2 \text{ GeV}$. The flux-integrated CCQE total cross section, obtained by integrating the double differential one over this range was measured to be $18.447 \times 10^{-39} \text{ cm}^2$ and $9.429 \times 10^{-39} \text{ cm}^2$ for range $-1 < \cos\theta < 1$, $0 < T < 2 \text{ GeV}$. The total normalization error on this measurement is 10.7%. These results contain the most complete and model-independent information that is available from experiment on the CCQE process.

We calculated the flux-integrated double differential cross section $(d^2\sigma/dTd\cos\theta)^{int}$ for the BNB ν_{mu} flux within the RDWIA and RFGM models with the extracted values of M_A using the T and Q^2 -bins similar to Ref. [29]

$$\left(\frac{d^2\sigma}{dTd\cos\theta}\right)_{ij}^{int} = \frac{1}{\Delta T \Delta \cos\theta} \int_{T_i}^{T_{i+1}} \int_{(\cos\theta)_j}^{(\cos\theta)_{j+1}} \left[\frac{d^2\sigma}{dTd\cos\theta}(T, \cos\theta)\right]^{int} dTd\cos\theta, \quad (22)$$

where $\Delta T = T_{i+1} - T_i = 0.1 \text{ GeV}$ and $\Delta \cos\theta = (\cos\theta)_{j+1} - (\cos\theta)_j = 0.1$.

Figures 4 and 5 show measured flux-integrated $d^2\sigma/dTd\cos\theta$ cross sections as functions of $\cos\theta$ for several bins of muon kinetic energy in the range $0.2 \leq T \leq 2 \text{ GeV}$ as compared with the RDWIA and RFGM calculations. There is good agreement between the RDWIA calculations and data within the error of the experiment. But in the regions $0.2 \leq T \leq 0.3 \text{ GeV}$, $-1 \leq \cos\theta \leq -0.3$ and $0.2 \leq T \leq 0.5 \text{ GeV}$, $0.9 \leq \cos\theta \leq 1$ the RDWIA result are slightly lower than measured cross section and the difference decreases with muon energy.

The RFGM prediction also agree well with data within the errors, except the region $0.7 < \cos\theta < 1$ and $0.2 < T < 0.5 \text{ GeV}$, where the calculated cross sections fall down rapidly with $\cos\theta$. In this kinematic region the Fermi gas model underestimates the double

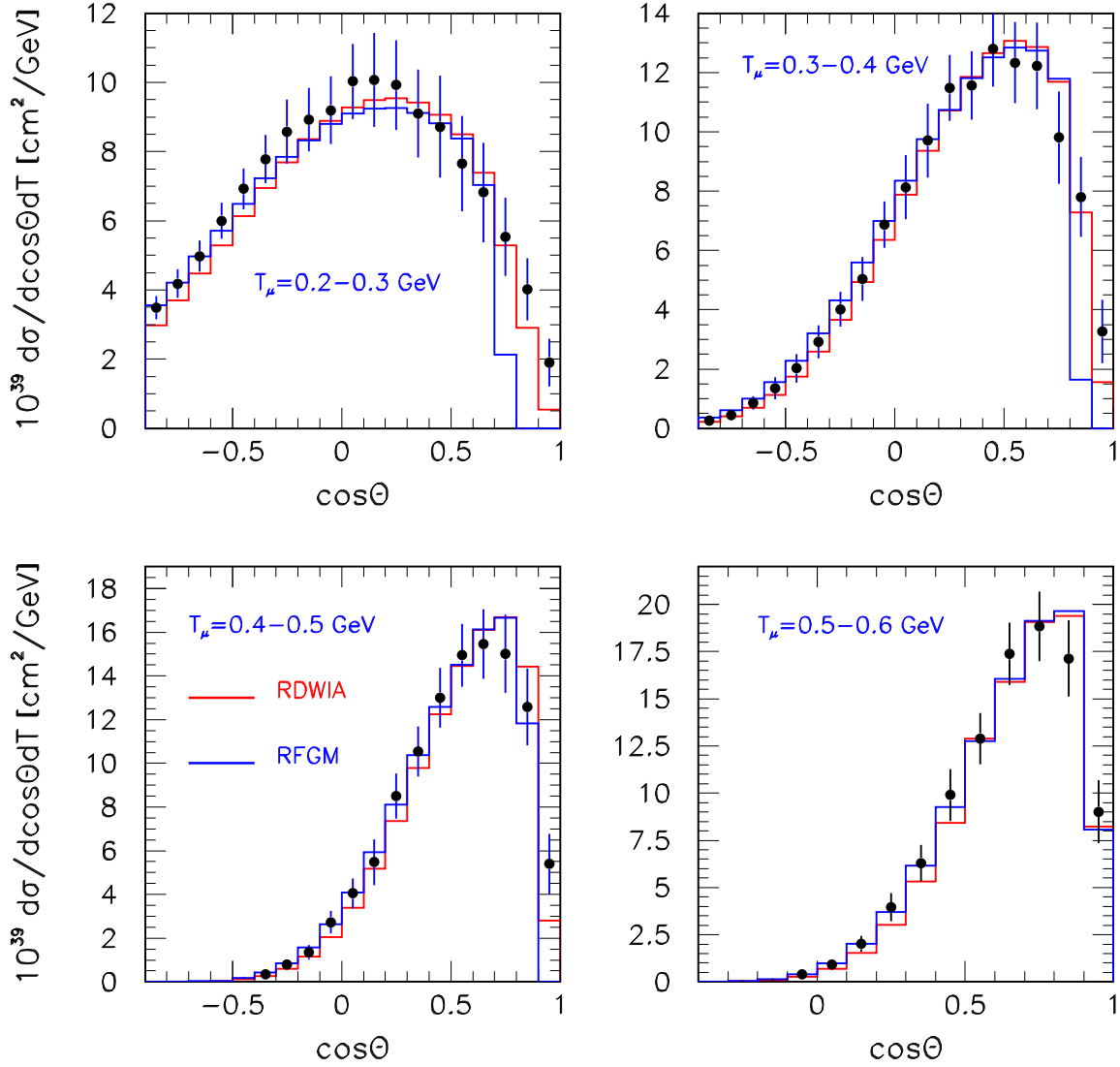


FIG. 4: (Color online) Flux-integrated $d^2\sigma/dTd\cos\theta$ cross section per neutron target for the ν_μ CCQE process as a function of $\cos\theta$ for the four muon kinetic energy bins: $T(\text{GeV})=(0.2 - 0.3)$, $(0.3 - 0.4)$, $(0.4 - 0.5)$, and $(0.5 - 0.6)$. As shown in the key, cross sections were calculated within the RDWIA ($M_A = 1.37 \text{ GeV}/c^2$) and RFGM ($M_A = 1.36 \text{ GeV}/c^2$). The MiniBooNE data are shown as points with the shape error only.

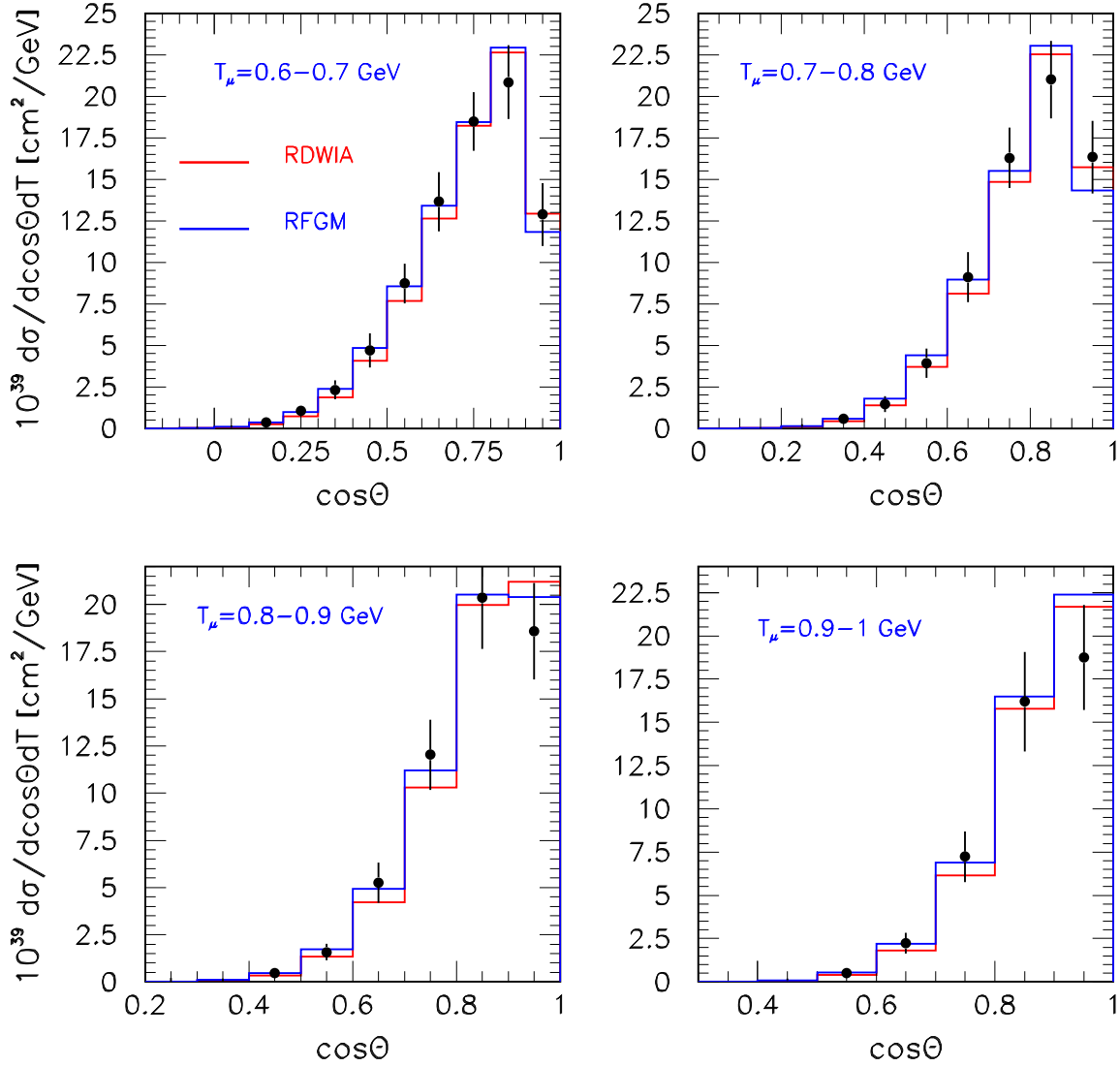


FIG. 5: (Color online) Same as Fig. 4 but for muon kinetic energy bins: $T(\text{GeV})=(0.6 - 0.7)$, $(0.7 - 0.8)$, $(0.8 - 0.9)$, and $(0.9 - 1)$.

differential cross section significantly. This trend is characteristic of nucleon momentum distribution and Pauli blocking effect as calculated in the Fermi gas model [47].

Figure 6 shows measured flux-integrated $d^2\sigma/dTd\cos\theta$ cross sections as functions of muon energy for four bins of muon scattering angle as compared with the RDWIA and RFGM

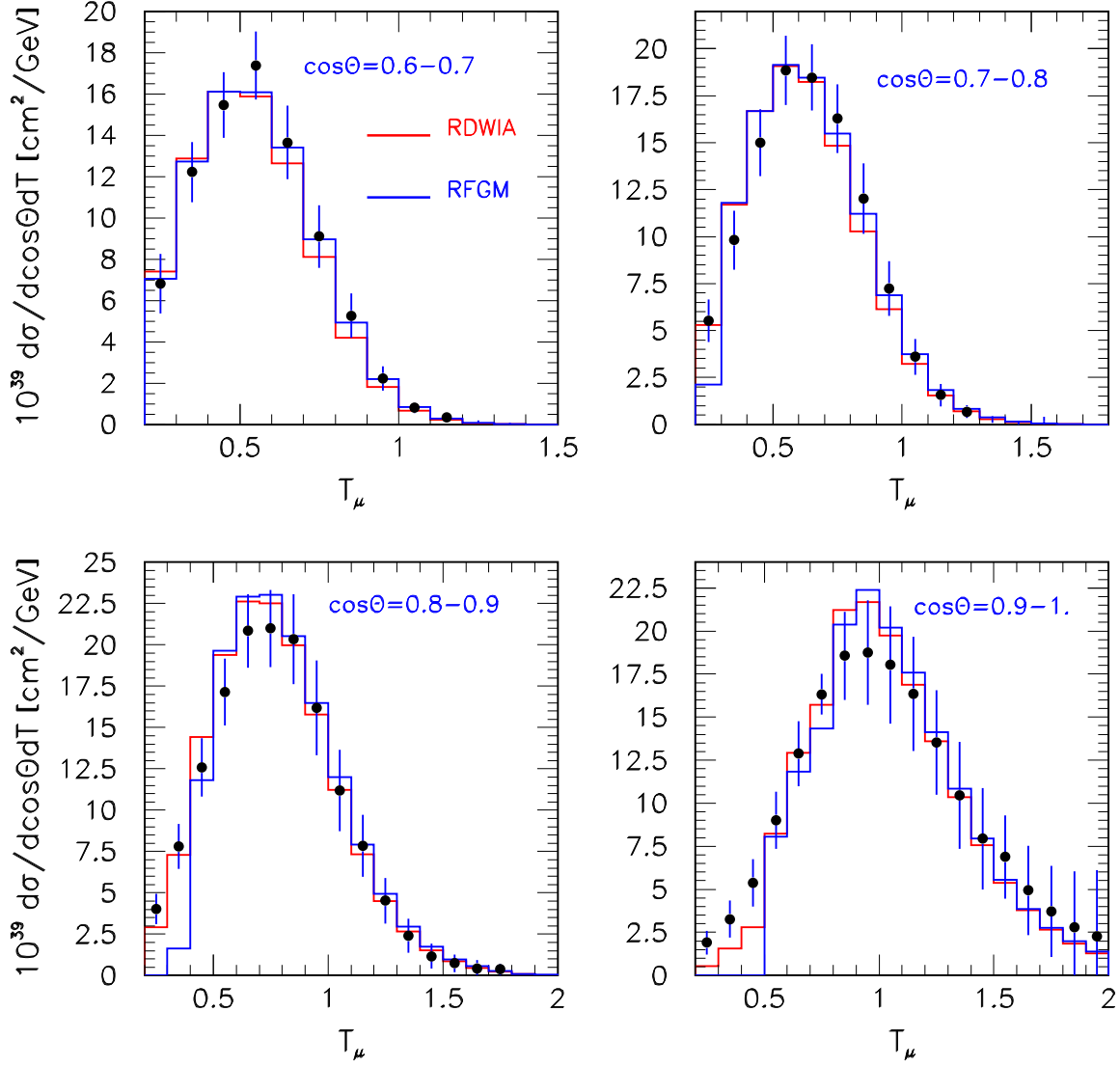


FIG. 6: (Color online) Flux-integrated $d^2\sigma/dT d\cos\theta$ cross section per neutron target for the ν_μ CCQE process as a function of muon energy for the four muon scattering angle bins: $\cos\theta=(0.6 - 0.7)$, $(0.7 - 0.8)$, $(0.8 - 0.9)$, and $(0.9 - 1)$. As shown in the key, cross sections were calculated within the RDWIA ($M_A = 1.37 \text{ GeV}/c^2$) and RFGM ($M_A = 1.36 \text{ GeV}/c^2$). The MiniBooNE data are shown as points with the shape error only.

calculations. Apparently that the RDWIA cross sections are lower than the measured ones in the kinematic region $0.9 < \cos \theta < 1$, $0.2 \leq T \leq 0.5$ (GeV) and the RFGM calculation underestimates the measured double differential cross section significantly in the range $0.7 < \cos \theta < 1$, $0.2 < T < 0.5$ GeV.

So, the comparison measured and calculated flux-integrated $d^2\sigma/dT d\cos\theta$ cross sections shows that the Fermi gas model prediction are completely off the data in the range $0.7 < \cos \theta < 1$, $0.2 < T < 0.5$ GeV. The RDWIA cross sections underestimate the measured ones for muon production with energies $T \leq 0.3$ GeV and scattering angles $\cos \theta > 0.9$.

C. CCQE flux-integrated $d\sigma/dT$ and $d\sigma/d\cos\theta$ cross section

The flux-integrated single differential cross sections $d\sigma/dT$ and $d\sigma/d\cos\theta$ (for $T \geq 0.2$ GeV) are presented in Fig. 7, which shows $d\sigma/dT$ as a function of kinetic muon energy and $d\sigma/d\cos\theta$ as a function of muon scattering angle. Here the results obtained in the RDWIA and Fermi gas models compared with the MiniBooNE data. The measured flux-integrated $d\sigma/dT$ ($d\sigma/d\cos\theta$) cross section with the shape error has been obtained by summing the double differential one over $\cos\theta$ -bins (T -bins) presented in Tables VI and VII in Ref. [29]. There is a good agreement between the calculated and measured cross sections, with the exception of the bin $0.2 \leq T \leq 0.3$ GeV. The flux integrated total cross sections obtained in the RDWIA and RFGM approaches by integrating the double differential cross sections (over $-1 \leq \cos \theta \leq 1$, $0.2 \leq T \leq 2$ GeV), are equal of 8.208×10^{-39} cm² and 8.310×10^{-39} cm², correspondingly, and agree with measured one of 8.447×10^{-39} cm².

D. CCQE total cross section

The MiniBooNE flux-unfolded CCQE cross section per neutron as a function of neutrino energy is shown in Fig. 8 together with data of Refs. [48–51]. Also shown for comparison are the results obtained in the RDWIA, PWIA, and RFGM approaches. The calculated cross sections with the values of M_A , extracted from the shape-only fit to the flux-integrated $d\sigma/Q^2$ data reproduce the MiniBooNE total cross section within the errors of experiment over the entire measured energy range. At the average energy of the MiniBooNE flux (≈ 800 MeV), the extracted cross section is $\approx 30\%$ higher than what is commonly assumed for this process

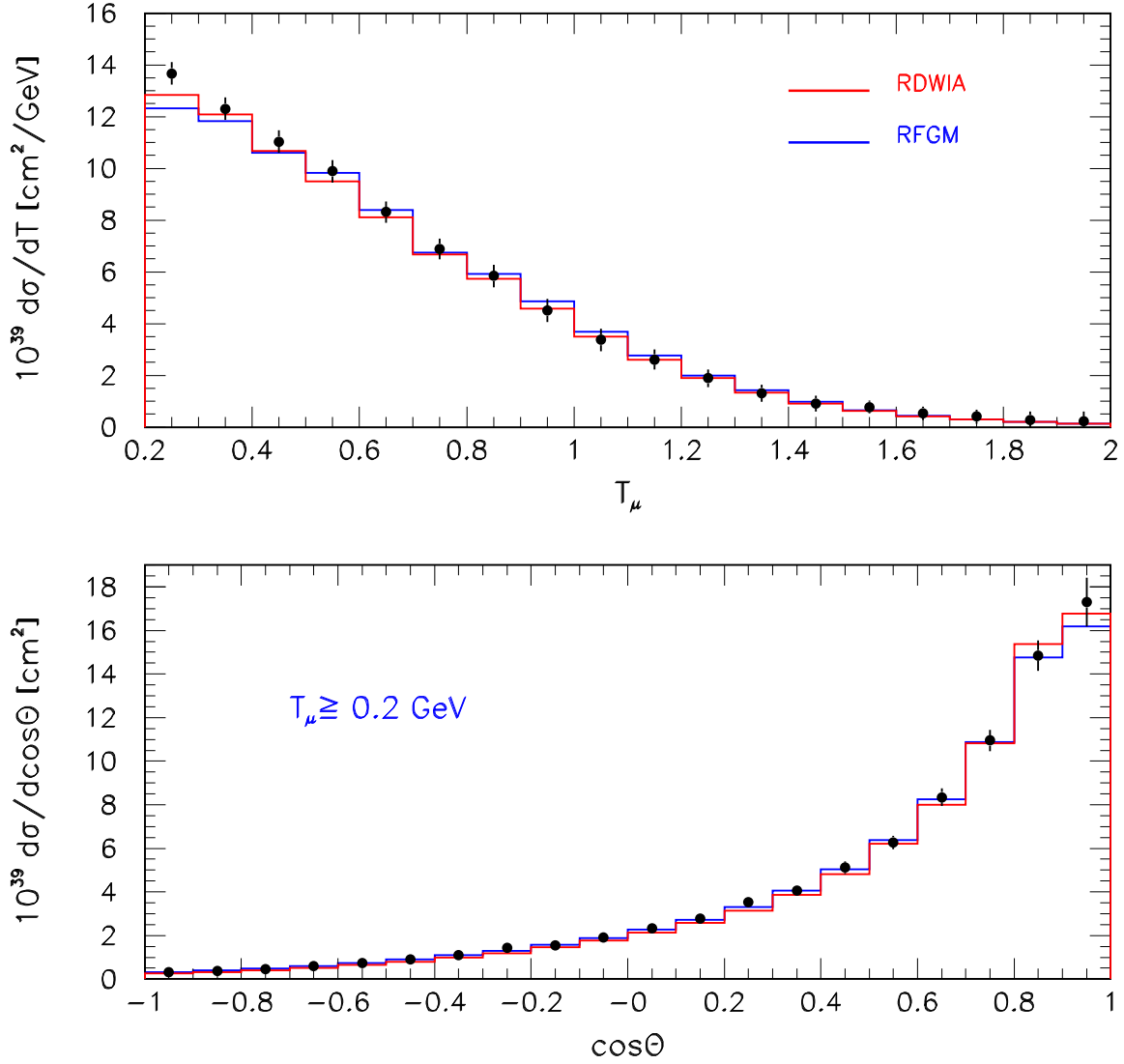


FIG. 7: (Color online) Flux-integrated $d\sigma/dT$ cross section as a function of muon energy (upper panel) and $d\sigma/d\cos\theta$ cross section for $T \geq 0.2$ GeV as a function of muon scattering angle (lower panel) for the ν_μ CCQE process. As shown in the key, cross sections were calculated within the RDWIA and RFGM. The MiniBooNE data are shown as points with the shape error only.

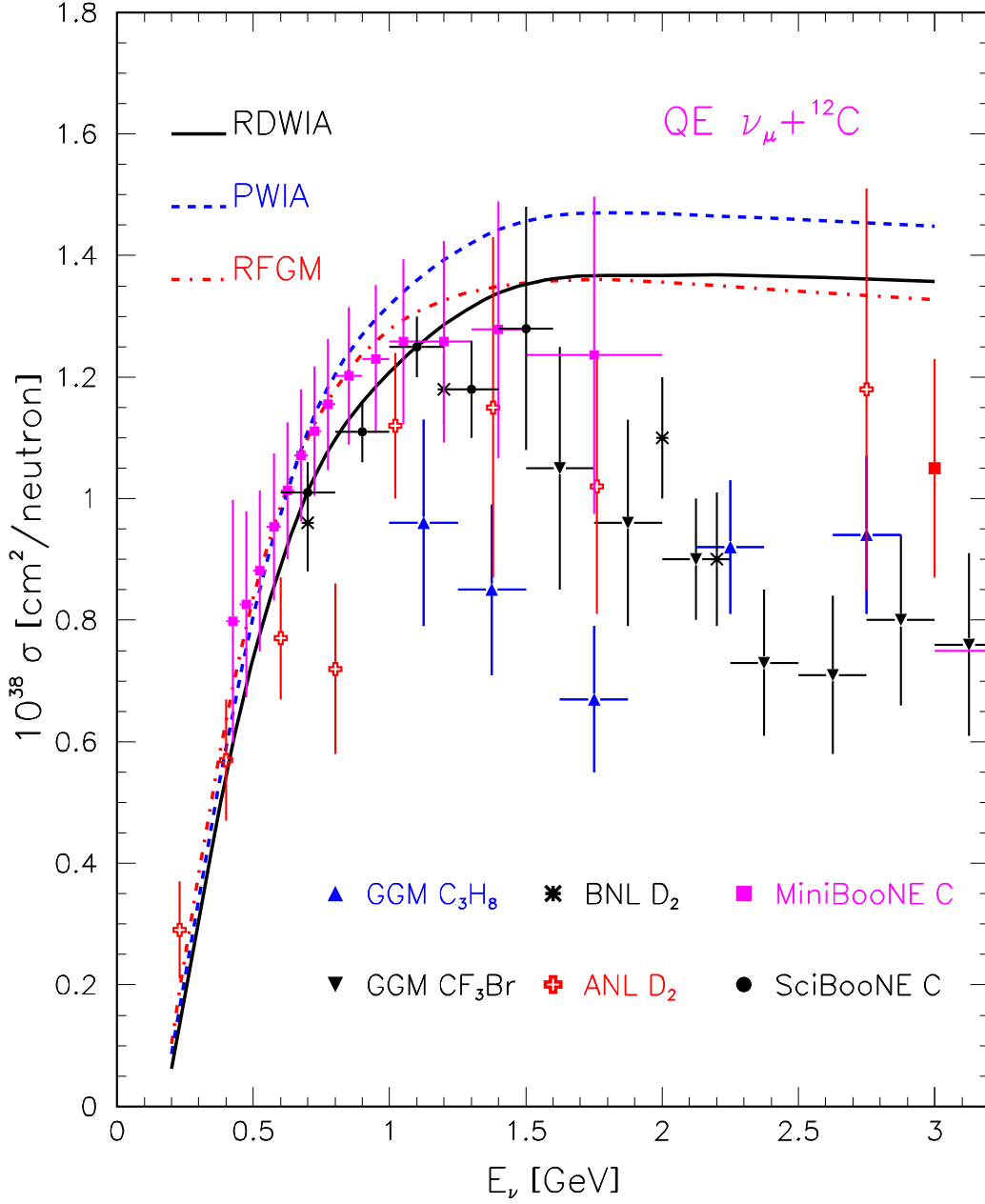


FIG. 8: (Color online) Total ν_μ CCQE cross section per neutron as a function of neutrino energy. Data points for different targets are from [26, 29, 48–51]. Also shown are predictions of the RDWIA ($M_A = 1.37 \text{ GeV}/c^2$), PWIA ($M_A = 1.37 \text{ GeV}/c^2$), and RFGM ($M_A = 1.36 \text{ GeV}/c^2$).

assuming the RFGM and world-average value of the axial mass, $M_A = 1.03 \text{ GeV}/c^2$. Note, that the spread in the data is much higher than a difference in predictions of the RDWIA, PWIA, and RFGM approaches. So, the comparison of the predicted and measured model-

independent flux-integrated double differential cross sections is more sensitive test of the employed models of the CCQE process than the comparison of the total cross sections.

IV. CONCLUSIONS

In this paper, we analyze the flux-averaged and flux-integrated differential and total ν_μ CCQE cross sections placing particular emphasis on their nuclear-model dependence. We found that the flux-integrated cross sections are model-independent and can be used to test of employed models of the CCQE interaction on nuclear targets. The flux-integrated double differential $d^2\sigma/dT d\cos\theta$, single differential $d\sigma/dQ^2$, $d\sigma/dT$, $d\sigma/d\cos\theta$, and flux-unfolded $\sigma(\varepsilon_i)$ CCQE cross sections were measured in the MiniBooNE experiment [29].

Using the RDWIA and RFGM approaches with the BNB flux we extracted an axial mass from a “shape-only” fit of the measured flux-integrated $d\sigma/dQ^2$ differential cross section. The extracted value of $M_A = 1.37 \pm 0.05$ GeV/c² (RDWIA) and $M_A = 1.36 \pm 0.05$ GeV/c² (RFGM) that is consistent with the MiniBooNE result of $M_A = 1.35 \pm 0.17$ GeV/c². The flux-integrated double differential cross sections were calculated in these models with extracted values of M_A . There is an overall agreement between the RDWIA result and data, whereas the RFGM calculation overestimates the measured cross section at $Q^2 < 0.2$ (GeV/c)². Thus, so-called low- Q^2 problem is successfully solved in the framework of RDWIA.

We also calculated in the RDWIA and RFGM approaches the flux-integrated $d^2\sigma/dT d\cos\theta$, $d\sigma/dQ^2$, $d\sigma/dT$ (for muons with kinetic energy $T \geq 0.2$ GeV), and total cross sections and compared them with the MiniBooNE data. The comparison of the RDWIA double differential cross section shows good agreement with data within the error of the experiment, except in the region $0.2 \leq T \leq 0.3$ GeV, $0.9 \leq \cos\theta \leq 1$ where the calculated cross sections are lower than measured ones. A good agreement between the RFGM calculation and data is observed exclusive of the range $0.7 \leq \cos\theta < 1$, $0.2 \leq T \leq 0.5$ GeV where the Fermi gas model predictions are completely off of the data. The calculated $d\sigma/dT$ and $d\sigma/d\cos\theta$ also describe well the measured cross sections except the muon energy bin $0.2 \leq T \leq 0.3$ GeV where the calculations are lower than the data.

The calculated and measured flux-integrated total cross sections are match well. The RDWIA, PWIA and RFGM calculations with extracted values of M_A reproduce the MiniBooNE

flux-unfolded CCQE cross section within the experimental error over the entire measured energy range.

We conclude that the flux-integrated double differential cross section which is model-independent should be used as the preferred choice for comparison to employed model of the CCQE interaction on nuclear targets.

Acknowledgments

The author greatly acknowledges S. Kulagin, J. Morfin, G. Zeller, and T.Katori for fruitful discussions at different stages of this work.

-
- [1] A. A. Aguilar-Arevalo *et al.*, (MiniBooNE Collaboration), Phys. Rev. Lett. **100**, 032301 (2008).
 - [2] P. Adamson *et al.*, (MINOS Collaboration), Phys. Rev. **D77**, 072002 (2008).
 - [3] A. Ferrero *et al.*, (T2K Collaboration), AIP Conf. Proc., **1189**, 77 (2009).
 - [4] G. Rosa *et al.*, (OPERA Collaboration), Nucl. Phys. B (Proc. Suppl.) **145**, 98 (2005).
 - [5] D. S. Ayres *et al.*, (NOvA Collaboration), arXiv:hep-ex/0503053.
 - [6] K. S. McFarland *et al.*, (MiNERvA Collaboration), Nucl. Phys. B (Proc. Suppl.) **159**, 107 (2006).
 - [7] M. Soderberg *et al.*, (MicroBooNE Collaboration), AIP Conf. Proc. **1189**, 83 (2009).
 - [8] R. A. Smith and E. J. Moniz, Nucl. Phys. **B43**, 605 (1972); *erratum: ibid.* **B101**, 547 (1975).
 - [9] A. Kim, J. Piekazewicz, C. J. Horowitz, Phys. Rev. **C51**, 2739 (1995).
 - [10] J. Nieves, M. Valverde, and M. J. Vicente Vacas, Phys. Rev. **C73**, 025504 (2006). 1
 - [11] A. Meucci, C. Giusti, and F. D. Pacati, Nucl. Phys. **A739**, 277 (2004).
 - [12] C. Maieron, M. C. Martinez, J. A. Caballero, and J. M. Udias, Phys. Rev. **C68**, 048501 (2003).
 - [13] M. C. Martinez, P. Lava, N. Jachowicz, J. Ryckebusch, K. Vantournhout, and J. M. Udias, Phys. Rev. **C73**, 024607 (2006).
 - [14] K. S. Kim, M. K. Cheoun, and B. G. Yu, Phys. Rev. **C77**, 054604 (2008).
 - [15] M. S. Athar, S. Chauhan, S. K. Singh, and M. J. Vicente Vacas, arXiv:0808.1437 [nucl-th].
 - [16] T. Leitner, O. Buss, L. Alvarez-Ruso, and U. Mozel, Phys. Rev. **C79**, 034601 (2009)

- [17] M. Martini, M. Ericson, G. Marteau , Phys. Rev. **C80**, 065501 (2009)
- [18] A. V. Butkevich and S. A. Kulagin, Phys. Rev. **C76**, 045502, (2007).
- [19] A. V. Butkevich, Phys. Rev. **C80**, 014610, (2009).
- [20] S. Boyd, S. Dytman, E. Hernandez, and R. Tacik , AIP Conf. Proc. **1189**, 60 (2009)
- [21] K. S. Kuzmin, V. V. Lyubushkin, and V. A. Naumov Eur. Phys. J. **C54**, 517, (2008).
- [22] V. Bernard, L. E. Elouadrhiri, U. -G. Meissner J. Phys. **G28**, R1, (2002).
- [23] V. Lyubushkin *et al.*, (NOMAD Collaboration), Eur. Phys. J. **C63**, 355, (2009).
- [24] R. Gran *et al.*, (K2K Collaboration), Phys. Rev. **D74**, 052002 (2006).
- [25] X. Espinal, F. Sanchez, AIP (Conf. Proc.) **967**, 117 (2007).
- [26] J. L. Alcaraz-Aunion and J. Walding (SciBooNE Collaboration), AIP Conf. Proc. **1189**, 145 (2009).
- [27] M. Dorman *et al.* (MINOS Collaboration) AIP Conf. Proc. **1189**, 133 (2009).
- [28] A. V. Butkevich and S. P. Mikheyev, Phys. Rev. **C72**, 025501 (2005).
- [29] A. A. Aguilar-Arevalo *et al.* (MiniBooNE Collaboration) arXiv:1002.2680 [hep-ex].
- [30] T. Katori *et al.* (MiniBooNE Collaboration) AIP Conf. Proc. **1189**, 139 (2009).
- [31] P. Mergell, U.-G. Meissner, and D. Drechsel, Nucl. Phys. **A596**, 367, 1996.
- [32] T. de Forest, Nucl. Phys. **A392**, 232, 1983.
- [33] D. Dutta *et al.*, Phys. Rev. **C68**, 064603, (2003).
- [34] J. J. Kelly Phys. Rev. **C71**, 064610 (2005).
- [35] B. Serot, J. Walecka, Adv. Nucl. Phys. **16**, 1, 1986.
- [36] C. J. Horowitz D. P. Murdock, and Brian D. Serot, in *Computational Nuclear Physics 1: Nuclear Structure* edited by K. Langanke, J. A. Maruhn, Steven E. Koonin (Springer-Verlag,Berlin, 1991), p.129
- [37] J. J. Kelly Phys. Rev. **C59**, 3256 (1999).
- [38] J. J Kelly, <http://www.physics.umd.edu/enp/jjkelly/LEA>
- [39] D. Rohe *et al.*, Nucl. Phys. B (Proc. Suppl.) **159**, 152 (2006).
- [40] E .D. Cooper, S. Hama, B. C. Clark, and R. L. Mercer, Phys. Rev. **C47**, 297 (1993).
- [41] K. G. Fissum *et al.*, Phys. Rev. **C70**, 034606, 2004
- [42] A. Meucci, C. Giusti, and F. D. Pacati, Nucl. Phys. **A744**, 307 (2004).
- [43] A. Meucci, F.Capuzzi, C. Giusti, and F. D. Pacati, Phys. Rev. **C67**, 054601 (2003).
- [44] S. A. Kulagin and R. Petti, Nucl. Phys. **A765**, 126, 2006.

- [45] Ciofi degli Atti and S. Simula, Phys. Rev. **C53** , 1689, 1996.
- [46] A. A. Aguilar-Arevalo *et al.*, (MiniBooNE Collaboration), Phys. Rev. **C79**, 072002 (2009).
- [47] A. V. Butkevich, Phys. Rev. **C78**, 015501 (2008).
- [48] W. A. Mann *et al.*, Phys. Rev. Lett. **31**, 844, (1973).
- [49] N. J. Baker *et al.*, Phys. Rev. **D23**, 2499, (1981).
- [50] M. Pohl *et al.*, Lett. Nuovo Cim. **26**, 332, 1979.
- [51] J. Brunner *et al.*, Z. Phys. **C45**, 551, 1990.